Turk J Pharm Sci 2026;23(3):174-186
DOI: 10.4274/tjps.galenos.2026.78567

ORIGINAL ARTICLE

Synthesis, Characterization, and *In Vitro* Anticancer Activity of Fe_3O_4-PEG-Quercetin Nanoparticles in a Non-Small Cell Lung Cancer (NSCLC) Model

Yeşim SİS[1]*, Mükerrem Betül YERER[2]

[1]Erciyes University, Ziya Eren Pharmaceutical Application and Research Center, Kayseri, Türkiye
[2]Erciyes University Faculty of Pharmacy, Department of Pharmacology, Kayseri, Türkiye

ABSTRACT

Objectives: Lung cancer is one of the leading causes of cancer-related mortality worldwide, with non-small cell lung cancer (NSCLC) accounting for the vast majority of cases. Conventional chemotherapeutic approaches are frequently limited by systemic toxicity, poor bioavailability, and non-selective biodistribution. Nanoparticle-based drug delivery systems have emerged as a promising strategy to overcome these limitations. The present study aimed to synthesize a novel PEGylated magnetite nanoparticle system containing quercetin (Fe_3O_4-PEG-QUER) and evaluate its effects on the impedance-based cellular responses of the A549 NSCLC cell line compared with non-tumorigenic bronchial epithelial cells (BEAS-2B).

Materials and Methods: Nanoparticles were synthesized via the coprecipitation method. Quercetin was introduced during the preparation of the Fe_3O_4-PEG formulation, resulting in the Fe_3O_4-PEG-QUER formulation. All formulations Fe_3O_4, Fe_3O_4-QUER, Fe_3O_4-PEG, and Fe_3O_4-PEG-QUER were characterized using X-ray diffraction, fourier-transform infrared spectroscopy, Zeta-sizer, and nanoparticle tracking analysis. Impedance-based cellular responses were assessed in BEAS-2B and A549 cell lines using the xCELLigence real-time cell analysis system.

Results: Fe_3O_4-PEG-QUER showed apparent antiproliferative effects against A549 cells, with IC50 values of 289 µg/mL at 24 h and 160 µg/mL at 48 h. For BEAS-2B cells, the apparent IC50 values were above the highest tested concentration (> 400 µg/mL) at the evaluated time points. Fe_3O_4-PEG alone showed marked effects on the impedance-based cellular response of A549 cells, with apparent IC50 values of 27 and 19 µg/mL at 24 and 48 h, respectively. Because quercetin loading was not quantitatively determined, the nanoparticle concentrations represent total formulation mass and cannot be directly converted to quercetin-equivalent doses.

Conclusion: Fe_3O_4-PEG-QUER nanoparticles altered the impedance-based cellular response in the A549 NSCLC cell line, with smaller changes observed in BEAS-2B cells at lower concentrations. These findings provide preliminary *in vitro* evidence supporting further investigation of Fe_3O_4-PEG-QUER in lung cancer models.

Keywords: Nanoparticles, A549, XRD, NTA and xCELLigence

***Correspondence:** yesimsis@erciyes.edu.tr, **ORCID-ID:** orcid.org/0009-0009-3108-7122

Received: 03.03.2026 **Accepted:** 15.10.2026 **Publication Date:** 27.10.2026

Cite this article as: Sis Y, Yerer MB. Synthesis, characterization, and *in vitro* anticancer Activity of Fe_3O_4-PEG-quercetin nanoparticles in a non-small cell lung cancer (NSCLC) model. Turk J Pharm Sci. 2026;23(3):174-186

Copyright© 2026 The Author(s). Published by Galenos Publishing House on behalf of Turkish Pharmacists' Association.
This is an open access article under the Creative Commons Attribution-NonCommercial-NoDerivatives 4.0 (CC BY-NC-ND) International License.

INTRODUCTION

Super-paramagnetism arises from the limited size of magnetic nanoparticles (MNP).[1] In biomedical applications, super-paramagnetic nanoparticles can be used, which become magnetic in the presence of a magnetic field but lose their magnetic properties when this field is removed.[2,3] Since MNP have a tendency to clump due to their high surface energy and magnetic interactions, the body perceives the nanoparticle as a foreign object and tries to get rid of it.[2] To prevent such problems, coatings such as polyethylene glycol (PEG), polyvinyl alcohol (PVA), dextran, carbohydrate and protein are used.[4-6] PEG is a hydrophilic, neutral, non-toxic, protein-resistant polymer with high surface fluidity.[7-12] Due to these properties, PEG was used as a surface coating agent in this study.

Inorganic nanoparticles, such as silica, gold, and iron-oxide, and organic nanoparticles, such as liposomes, polymeric nanoparticles, and micelles, are used as therapeutic nanoparticles. Since inorganic nanoparticles gave good results in preclinical studies, they are suitable for clinical use and have been approved for use in areas such as anemia treatment and thermal ablation of tumors.[13,14] In addition, while inorganic nanoparticles provide benefits in areas such as magnetic resonance imaging and individual drug use, organic nanoparticles can be used for hemostasis, gene therapy and cancer treatment.[15,16]

There are eight iron-oxide compounds known in nature, including the most well-known types such as magnetite, hematite, and maghemite; while magnetite has a face-centered cubic structure in blackish-brown color, hematite is red-brown in color, formed as a result of volcanic activity, and maghemite is formed as a result of the oxidation of magnetite.[17-19] Iron-oxide nanoparticle (IONP) can be synthesized by several methods including coprecipitation, hydrothermal synthesis, and microemulsion. IONP can be used for medical purposes such as replacement therapy for anemia,[20,21] and magnetic resonance imaging as a contrast agent.[22-24] In imaging cancer and pathological types, IONP can be detected based on their behavior in the magnetic field.[5]

Flavonoids are a diverse group of polyphenolic compounds whose names are derived from the Latin word flavus, meaning "yellow." They are widely distributed in fruits, vegetables, tea, and other plant-based foods and are involved in various biological processes in plants.[25,26] Flavonoids, which show effects such as anti-inflammatory, antimutagenic, antioxidant and anti-carcinogenic, are used in pharmaceutical and medical applications.[27-29] Some of the flavonoids, also known as secondary metabolites of plants, attract attention in medicine and agriculture because they contain bioactive compounds that can interfere with nucleic acids and proteins, show anti-microbial and pharmacological properties, and kill insects.[30] Flavonoids can also be used in areas such as butyrylcholinesterase, acetylcholinesterase, and BACE1 inhibition, prevention of atherosclerosis, insulin receptor activator, antithrombogenic, lipoxygenase inhibition, inhibition of H1N1 influenza disease and NDM-1 inhibition.[25]

Cancer is a disease that deeply affects the world, caused by an excessive proliferation in the number of cells as a result of uncontrolled division of cells.[31] While lung cancer is the most common type of cancer in men worldwide, it is the type of cancer that comes right after breast cancer in women.[32] Early diagnosis of cancer is of great importance in terms of treatment because the development of cancer can be limited by early diagnosis.[33] Growths and changes in organs can be detected with classical methods, but this process can take a long time because it must wait until thousands of cancer cells have formed, whereas, thanks to nanotechnology, it can be detected at much lower cell counts. Even if a cancer cell has formed, it is possible to diagnose it. Since nanoparticles have the ability to enter a single cancer cell, cancerous cells can be easily detected.[34] Furthermore, classical methods such as radiotherapy, surgery and chemotherapy used to treat cancer can also damage healthy cells and tissues and have toxic effects.[35] MNP provide health benefits owing to their many features, such as a stable structure, high compatibility with cells and tissues, and ease of synthesis. It has received considerable attention in studies within the field. These substances have been used for years, and some types have been approved by the European Medicines Agency and the Food and Drug Administration (FDA) and have been used to treat people.[36] Many clinically approved nanoparticles have been used for treatment purposes in various stages of some types of cancer; PEG-Doxil is the first medical nanomaterial approved by the FDA in 1995 and used in cancer treatment.[37]

In this study, the coprecipitation method was selected for the synthesis of the nanoparticle formulations. Fe_3O_4 was synthesized from $FeCl_2 \cdot 4H_2O$ and $FeCl_3 \cdot 6H_2O$ in air; quercetin and PEG were incorporated into the formulation, with PEG serving as a surface-modifying component. The intermediate and final formulations were characterized by X-ray diffraction (XRD), fourier-transform infrared spectroscopy (FT-IR), nanoparticle tracking analysis (NTA), Zeta-sizer, scanning electron microscopy (SEM), and energy-dispersive X-ray spectroscopy (EDX) to obtain complementary information on their physicochemical properties. The in *vitro* cellular responses to the formulations were subsequently evaluated in the A549 [non-small cell lung cancer (NSCLC)] and non-tumorigenic bronchial epithelial (BEAS-2B) cell lines using the xCELLigence real-time impedance-based monitoring system. The study therefore provides comparative physicochemical data and *in vitro* cellular-response data for Fe_3O_4, Fe_3O_4-PEG, Fe_3O_4-QUER, and Fe_3O_4-PEG-QUER- based formulations.

MATERIALS AND METHODS

Chemicals and reagents

All chemicals were used as received without further purification. The reagents employed in this study, along with their suppliers and purity grades, are summarized in Table 1.

Preparation of IONP

$FeCl_2.4H_2O$:$FeCl_3.6H_2O$ was taken in the ratio of 1:2;[38-43] $FeCl_2.4H_2O$ and $FeCl_3.6H_2O$ were added to the reaction vessel,

Table 1. Chemicals and reagents used in this study.

Chemical	Supplier	Purity/grade	CAS/notes
$FeCl_2 \cdot 4H_2O$	Supelco	For analysis	13478–10–9
$FeCl_3 \cdot 6H_2O$	Isolab	≥ 97%	10025–77–1
Quercetin	Merck	≥ 95% (HPLC)	117–39–5
PEG 1000	BLDpharm	⟩ 97%	25322–68–3
Ethanol	Isolab	≥ 99.9%	64–17–5
Ammonia solution	Supelco	25%, for analysis	1336–21–6
DMSO	PanReac	≥ 99.5%, cell culture grade	67–68–5
PBS tablets	Sigma	pH 7.2–7.6	–
DMEM (high glucose)	Sigma	Cell culture grade	A549 medium
RPMI-1640	Sigma	Cell culture grade	BEAS-2B medium

DMSO, dimethyl sulfoxide.

10 mL of pure water was added and placed in the oil bath on the magnetic stirrer set at 80 °C and 300 rpm. When 3 mL of 25% NH_3 was added to the reaction vessel after 15 minutes, the brown-toned reaction color turned into silvery black and it was observed that the substance condensed/precipitated at the bottom. After 15 minutes, the reaction was terminated and transferred to 50 mL falcon tubes, centrifuged at 3900 rpm-room temperature for 5 minutes, washed twice with pure water, and then left to dry in an oven set at 60 °C. The reaction pH was not measured or recorded during the original synthesis.

IONP-PEG synthesis

The IONP–PEG synthesis procedure was adapted from previously reported IONP–PEG formulations, particularly those described by Dorniani et al.[44] and Rosman et al.[45] In these studies, PEG was incorporated into magnetite-based formulations; Rosman et al.[45] reported one based on 0.2 g of dried IONP. The reported formulation conditions were scaled down and adapted for an *in situ* procedure in which PEG was introduced during the IONP synthesis rather than after isolation and drying of the nanoparticles. After 30 min of synthesis, 5 mL of a 10% (w/v) solution of PEG 1000, prepared by dissolving 0.5 g of PEG 1000 in 5 mL of ethanol, was added to the reaction mixture. The mixture was subsequently subjected to centrifugation, washing, and drying.

IONP-QUER synthesis

The IONP–quercetin synthesis procedure was adapted from previously reported magnetite–PEG–active compound formulations, particularly those described by Dorniani et al.[44] and Rosman et al.[45]; Dorniani et al.[44] reported a magnetite–PEG formulation containing 1% PEG and 2% gallic acid, whereas Rosman et al.[45] reported a related Fe_3O_4–PEG–gallic acid formulation based on 0.2 g of dried IONP. In the present study, the reported formulation conditions were scaled down and adapted for quercetin and for an *in situ* synthesis procedure. 0.0595 g $FeCl_2 \cdot 4H_2O$ and 0.140 g $FeCl_3 \cdot 6H_2O$ were added to 930 μL of purified water in a 30 mL glass vial. The vial was placed in a 100 mL conical flask and maintained at 80 °C and stirred at 300 rpm using a magnetic stirrer with an oil bath. After 15 min, 280 μL of 25% NH_3 solution was added. After an additional 15 min, 0.0625 g of quercetin was dissolved in 3125 μL of ethanol to prepare a 2% (w/v) quercetin solution, which was added directly to the reaction mixture. Stirring was continued for 1 h, after which the resulting reaction mixture was subjected to centrifugation, washing, and drying.

IONP-PEG-QUER synthesis

IONP was synthesized as described in the IONP-QUER synthesis, and 5 mL of a 1% (w/v) PEG 1000 solution (prepared by dissolving 0.05 g PEG 1000 in 5 mL of ethanol) was added after 30 minutes. After 1 hour, 0.0625 g of quercetin was dissolved in 3125 μL of ethanol to prepare a 2% (w/v) quercetin solution, which was then added to the reaction vessel. After 30 minutes, 350 μL of 25% NH_3 was added to the reaction vessel and the reaction was continued for another two and a half hours. At the end of this period, the reaction vessel was removed, centrifuged, washed, and dried (Figure 1).

Physicochemical characterization

All formulations were characterized by XRD for crystal structure and phase purity; FT-IR for verification of surface functionalization; dynamic light scattering (Zeta-sizer) for hydrodynamic size and zeta potential; NTA for size distribution and particle concentration; SEM for morphological evaluation; and EDX for elemental composition.

Cell culture conditions

A549 (ATCC CCL-185, NSCLC adenocarcinoma) and BEAS-2B (ATCC CRL-9609, non-tumorigenic bronchial epithelial cells) cell lines were used. A549 cells were maintained in DMEM (high glucose; Sigma) supplemented with 10% FBS and 1% penicillin-streptomycin. BEAS-2B cells were cultured in RPMI-1640 (Sigma) supplemented with 10% FBS and 1% penicillin-streptomycin. Both lines were maintained at 37 °C in a humidified 5% CO2 incubator. Cells were harvested by centrifugation at 1000 rpm for 5 minutes at 25 °C prior to the experiments.

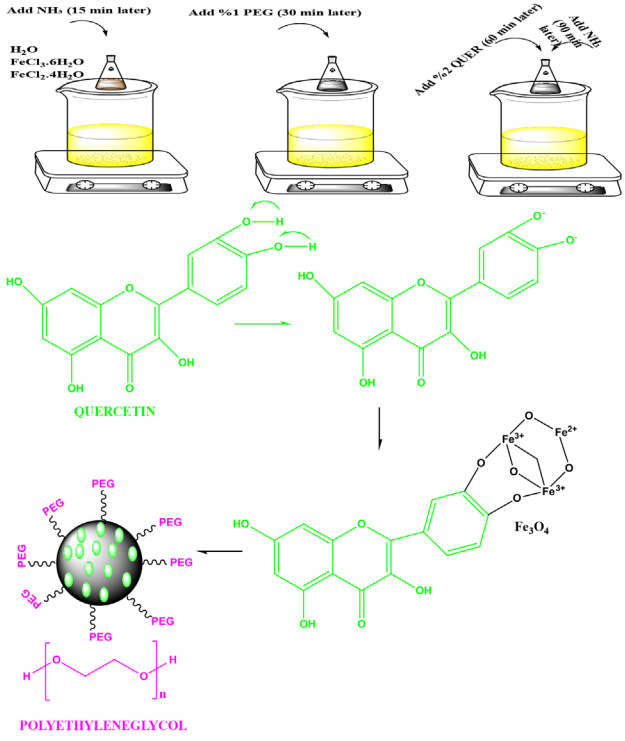


Figure 1. Experimental setup and schematic representation of IONP-PEG-QUER synthesis.

IONP, iron-oxide nanoparticle; QUER, quercetin.

Preparation of drug solutions

All formulations and free quercetin were prepared in dimethyl sulfoxide (DMSO) and in the appropriate culture medium (A549-DMEM/BEAS-2B-RPMI). Serial dilutions were performed in the appropriate culture medium to yield final concentrations of 12.5–400 µg/mL. After the prepared treatment solutions were added to the E-plate wells at a 1:1 volume ratio, the final DMSO concentration ranged from 0.5% at 400 µg/mL to 0.015625% at 12.5 µg/mL. A DMSO vehicle control was included in the experiments; however, concentration-matched vehicle controls were not included for each tested formulation concentration. Therefore, a possible contribution of the varying DMSO concentrations to the observed cellular responses cannot be fully excluded.

For experiments in which the cell index declined to approximately zero before 72 h, monitoring was terminated; therefore, a 72-h IC50 value was not determined and reported as N/D.

Impedance-based cellular response assessment (xCELLigence)

Cytotoxic effects were evaluated using the xCELLigence RTCA system (ACEA Biosciences/Agilent). A549 and BEAS-2B cells at the 5th passage were used for experiments. Cells were counted using a Bio-Rad cell counting device and seeded at a density of at least 10,000 cells per well in an xCELLigence E-plate (E-plate ID: 761460). Following cell seeding, impedance signals were monitored to establish the cellular baseline. The test formulations were applied at approximately 2 h and 22 h after cell seeding, according to the respective experimental setups. The treatment application times are also indicated in the corresponding xCELLigence graphs.

Fe_3O_4-PEG, Fe_3O_4-QUER, Fe_3O_4-PEG-QUER, and free quercetin were tested at concentrations of 12.5, 25, 50, 100, 200, and 400 µg/mL. Cellular responses were monitored for 48-72 h following treatment. At least three independent biological experiments were performed, each with two technical replicate wells for each tested concentration.

The xCELLigence RTCA system measures changes in electrical impedance associated with cellular attachment, spreading, proliferation, and other cellular responses; these changes are expressed as cell index values. Therefore, the cell index does not represent a direct measurement of cell viability. Apparent IC50 values were estimated separately at 24, 48, and 72 h using the corresponding cell index concentration–response data in the RTCA software. The concentration–response data were fitted to a sigmoidal dose–response model using DRC analysis (cell index at a time point vs. concentration). The curve settings were selected according to the concentration–response profile and goodness of fit. The resulting IC50 values were exported to GraphPad Prism 8.0.2 for statistical analysis. The corresponding culture medium was used as the control medium for each cell line: DMEM for A549 cells and RPMI-1640 for BEAS-2B cells. DMSO vehicle controls were also included in the experiments. These controls were included in the recorded RTCA data, and no separate manual normalization of cell index values was performed before IC50 analysis.

Statistical analysis

The xCELLigence results were calculated using RTCA software. For additional statistical evaluation, the data were analyzed using GraphPad Prism (version 8.0.2; GraphPad Software, San Diego, CA, USA). One-way analysis of variance, followed by Tukey's multiple comparisons test, was used for statistical comparisons. Each experimental condition was measured in technical duplicate wells. A p-value < 0.05 was considered statistically significant.

Ethics

There are no circumstances requiring ethics committee approval for this study.

Since only *in vitro* experiments were conducted within the scope of this study, patient consent was not required.

RESULTS

FT-IR

The FT-IR spectra of Fe_3O_4, Fe_3O_4-PEG, Fe_3O_4-QUER, and Fe_3O_4-PEG-QUER nanoparticles are shown in Figure 2a. While the O-H bond peak was observed in the 3000-3232 range[39] the Fe-O bond in the iron-oxide structure gave a peak in the 540-555 cm^{-1} range.[40] The C = O bond from quercetin in the 1651 cm^{-1} range,[38] while the CH_2 peak at 1344-1375 cm^{-1} and the C-C-O/C-O-H peak at 987-1056 cm^{-1} were observed. The C-H peak gave a peak of 833-871 cm^{-1} and the C = C aromatic ring peak of 1589-1612 cm^{-1}.[40,43]

XRD analysis

In the Fe_3O_4 structure, 30, 35, 43, 53, 57 and 62 2Θ values are respectively (HighScore Plus-ICPDS No: 88–0315); Bragg reflections were determined as 220, 311, 400, 422, 511, 440 and it was observed that the cubic crystal structure of IONP was formed.[44] The addition of PEG and quercetin during the preparation process did not result in an apparent loss of the characteristic cubic crystal structure of Fe_3O_4 (Figure 2b).

NTA

One mg of Fe_3O_4, Fe_3O_4-PEG, Fe_3O_4-QUER and Fe_3O_4-PEG-QUER was weighed and dissolved in 2000 µL ethanol and size analyses were performed on the NTA device (ethanol was chosen because it is a good solvent for quercetin). Measurements were made in three repetitions and the average was taken as basis. According to NTA analysis, the average size of IONPs is 99.1 nm. Since the number of particles with a size of 54.6 nm was high, iron-oxide gave the strongest peak at this point. The size distribution is not homogeneous (Figure 3a). When coated with iron-oxide PEG, an increase in size was observed and the average size increased to 170.5 nm as the polymer was attached to the structure (Figure 3b). For the formulation containing quercetin, the particle size decreased (average size: 66.6 nm) (Figure 3c). When PEG was present in the iron-oxide–quercetin formulation, the particle size increased compared to the structure of iron-oxide-quercetin. However, its size remained between 1–100 nm where nanoparticles are found (Figure 3d).

Zeta potential analysis

While 1 mg of Fe_3O_4, Fe_3O_4-PEG and Fe_3O_4-PEG-QUER was weighed and dissolved in 1000 µL of ethanol and given to the device, 1 mg of Fe_3O_4-QUER was also weighed and dissolved in 2000 µL of ethanol and given to the device. Zeta potential measurements were performed in triplicate under room-temperature conditions using a Malvern Zeta-sizer. The reported zeta potential values represent the mean of the three repeated measurements. The "Zeta Deviation" values represent the standard deviation of the zeta potential distribution reported by the instrument software and do not represent the variability between repeated measurements (Figure 4a-d).

Zeta potential measurements are summarized in Table 2. Bare Fe_3O_4 carried a negative surface charge (-9.74 mV). PEGylation shifted the surface charge to near-neutrality (+0.183 mV), consistent with the electrically neutral nature of PEG and its established charge-shielding effect. The formulation containing quercetin exhibited a more negative surface charge (-14.0 mV for Fe_3O_4-QUER), attributable to the phenolic hydroxyl groups of quercetin. The Fe_3O_4-PEG-QUER formulation exhibited an intermediate charge of -8.18 mV.

SEM images

The morphology of the synthesized Fe_3O_4-PEG-quercetin nanoparticles was analyzed using SEM. Figures 5a-d present SEM images and particle-size distributions of functionalized magnetite nanoparticles, both with and without quercetin. The particles exhibited sizes predominantly in the 100–200 nm range. A predominantly spherical morphology was observed; however, some degree of particle agglomeration was also evident in the SEM images.

EDX analysis

Elemental analysis was performed to determine the presence of expected elements in the synthesized formulations and to evaluate their elemental percentages. Elemental analysis was performed to determine the presence of expected elements in the synthesized formulation and to evaluate their elemental percentages. The Fe peak confirmed the presence of Fe_3O_4 in the formulation (Figure 6a). In formulations containing PEG and quercetin, relative iron percentages decreased, which may be attributable to these components (Figure 6b-d).

Impedance-based cellular response (xCELLigence)

The cellular responses to all formulations were evaluated at concentrations ranging from 12.5 to 400 µg/mL using the xCELLigence system (Figure 7). Cellular responses were

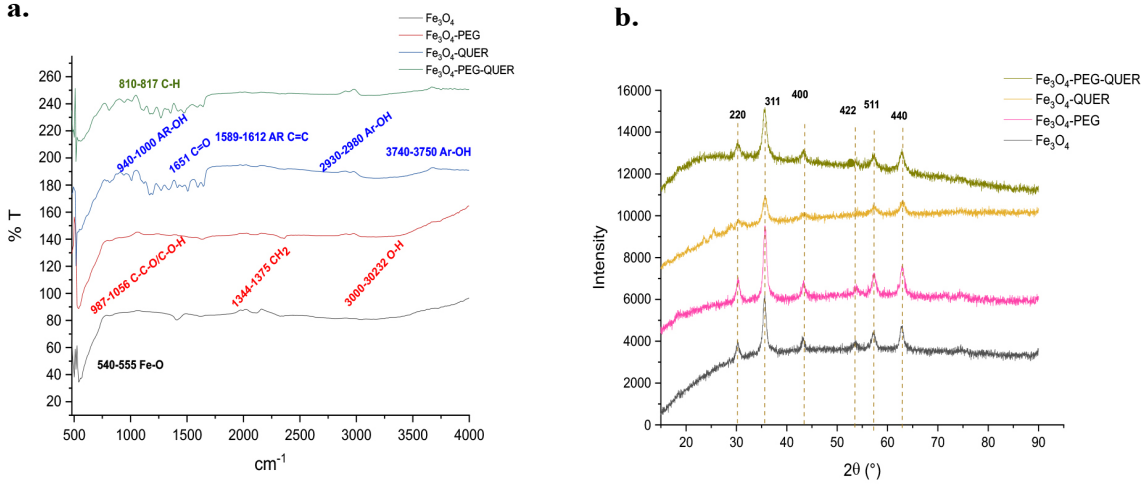


Figure 2. a. FT-IR spectra- 400–4000 cm^{-1}; **b.** XRD graph.

FT-IR, fourier-transform infrared spectroscopy; XRD, X-ray diffraction; QUER, quercetin.

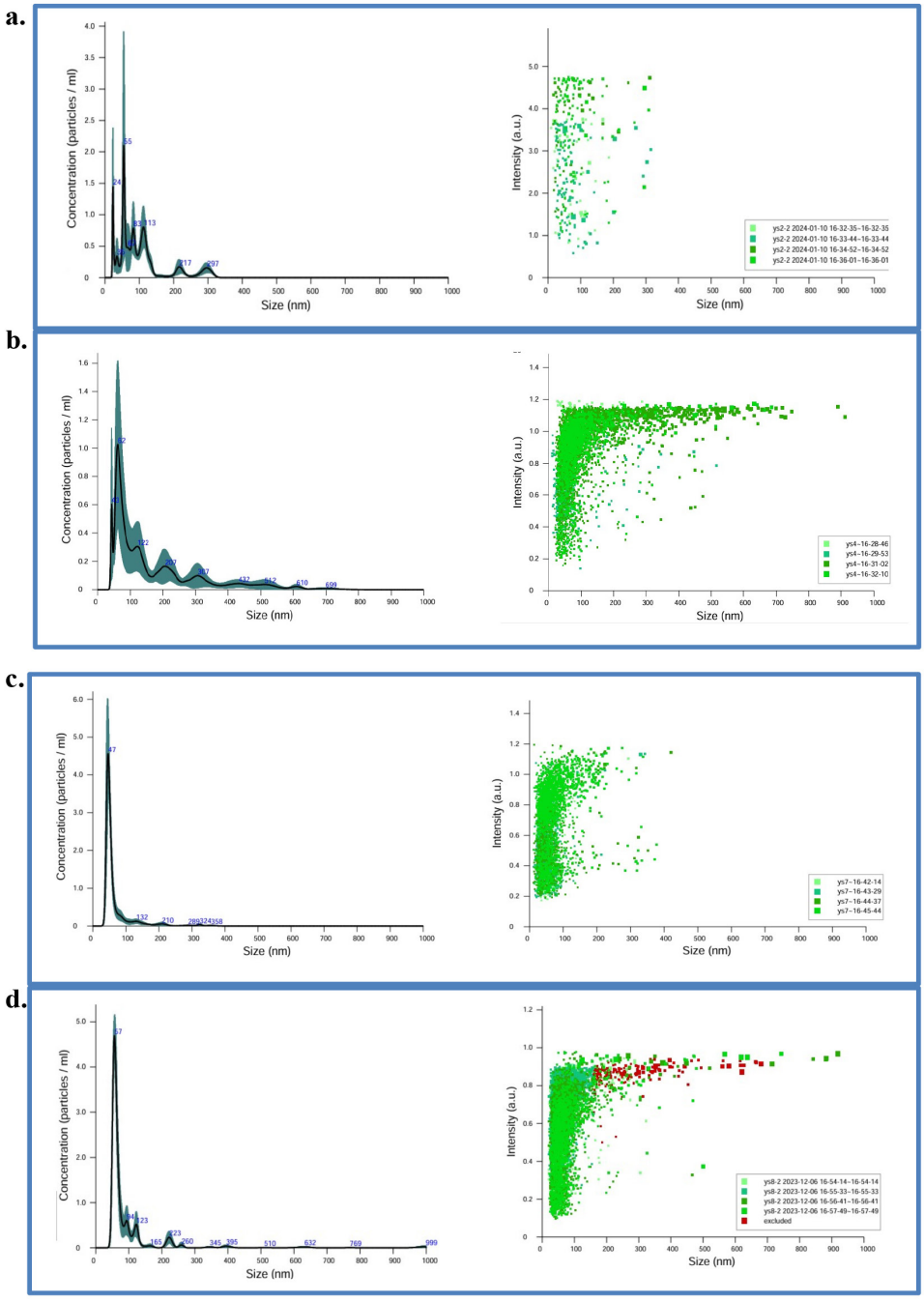


Figure 3. a. NTA result for Fe_3O_4 (mean particle size: 99.1 nm; strongest peak: 54.6 nm); **b.** NTA result for Fe_3O_4-PEG (mean particle size: 170.5 nm; strongest peak: 61.1 nm); **c.** NTA result for Fe_3O_4-QUER (mean particle size: 66.6 nm; strongest peak: 46.2 nm); **d.** NTA result for Fe_3O_4-PEG-QUER (mean particle size: 96.8 nm; strongest peak: 56.6 nm).

NTA, nanoparticle tracking analysis; QUER, quercetin.

monitored for 48–72 h, depending on the response profile. IC50 values determined at 24, 48, and 72 h are summarized in Table 3. Statistical comparisons between the tested conditions and untreated controls were significant ($p < 0.0001$).

Free quercetin exhibited significant cytotoxic activity at low concentrations (approximately 25 µg/mL) in both BEAS-2B and A549 (NSCLC) cell lines. Fe_3O_4-PEG exhibited cytotoxic activity in A549 cells (IC50 values: 27 and 19 µg/mL at 24 and 48 h, respectively), whereas higher concentrations were required to elicit a comparable response in BEAS-2B cells (IC50 values: 394, 394, and 360 µg/mL at 24, 48, and 72 h, respectively). These findings indicate that Fe_3O_4-PEG has greater cytotoxic activity in A549 cells than in non-tumorigenic BEAS-2B cells under the tested conditions.

In contrast, Fe_3O_4-PEG-QUER showed IC50 values above the highest tested concentration (› 400 µg/mL) in BEAS-2B cells at 24, 48, and 72 h. In A549 cells, Fe_3O_4-PEG-QUER exhibited cytotoxic activity at relatively low concentrations, with IC50 values of 289 and 160 µg/mL at 24 and 48 h, respectively. Thus, compared with free quercetin, Fe_3O_4-PEG-QUER showed lower cytotoxic activity in BEAS-2B cells while retaining measurable cytotoxic activity in A549 cells under the tested conditions.

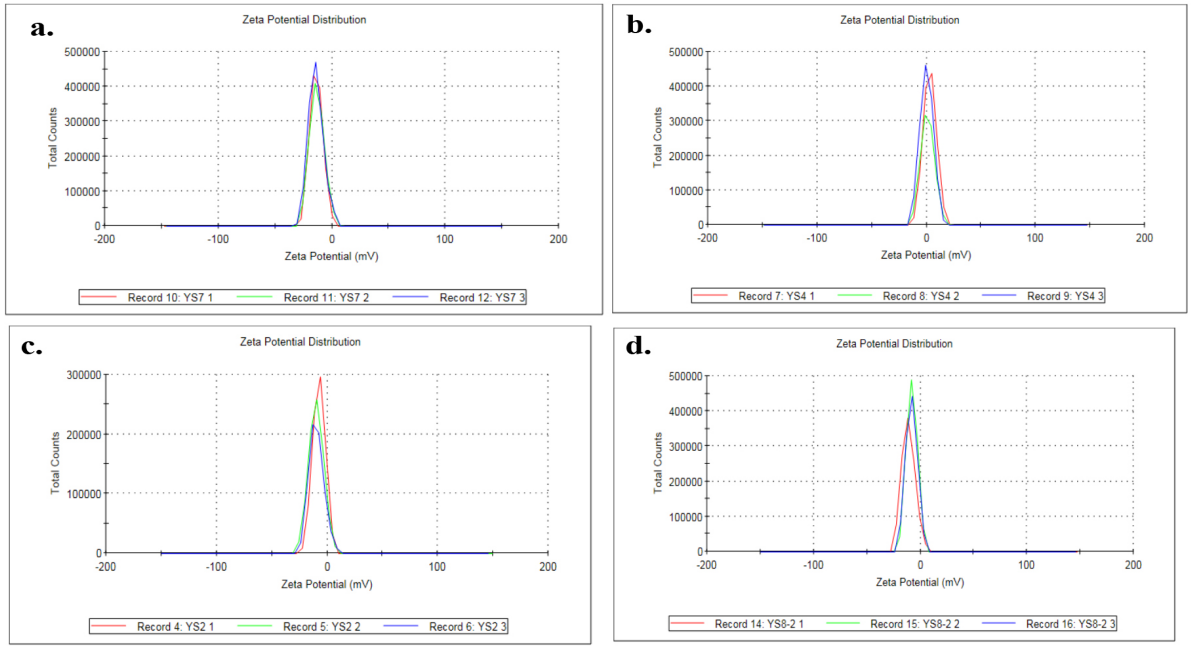


Figure 4. a. Fe_3O_4; **b.** Fe_3O_4-PEG; **c.** Fe_3O_4-QUER; **d.** Fe_3O_4-PEG-QUER zeta potential graph.
QUER, quercetin.

Table 2. Zeta potential results of the synthesized nanoparticle formulations based on three repeated measurements.

Formulation	Zeta potential (mV)	Zeta deviation (mV)	Charge
Fe_3O_4 (IONP)	-9.74	6.66	Negative
Fe_3O_4-PEG	+0.183	5.97	Near-neutral
Fe_3O_4-QUER	-14.0	6.52	Negative
Fe_3O_4-PEG-QUER	-8.18	5.35	Negative

QUER, quercetin.

Table 3. Apparent IC50 values (µg/mL) derived from xCELLigence cell index concentration-response data for all formulations in BEAS-2B and A549 cells at 24, 48, and 72 h.

Formulation	BEAS-2B				A549 (NSCLC)			
	IC50 24h	IC50 48h	IC50 72h	*p*-value	IC50 24h	IC50 48h	IC50 72h	*p*-value
Fe_3O_4-PEG	394 µg/mL	394 µg/mL	360 µg/mL	$p < 0.0001$	27 µg/mL	19 µg/mL	N/D*	$p < 0.0001$
Fe_3O_4-QUER	› 400	170 µg/mL	363 µg/mL	$p < 0.0001$	161 µg/mL	182 µg/mL	N/D*	$p < 0.0001$
Fe_3O_4-PEG-QUER	› 400	› 400	› 400	$p < 0.0001$	289 µg/mL	160 µg/mL	N/D*	$p < 0.0001$
QUER	25 µg/mL	25 µg/mL	24 µg/mL	$p < 0.0001$	25 µg/mL	25 µg/mL	134 µg/mL	$p < 0.0001$

*N/D: Not determined. IC50 values were determined from the corresponding cell index concentration-response data at 24, 48, and 72 h after treatment. Values › 400 µg/mL indicate that the IC50 was not reached within the tested concentration range. N/D indicates that the cell index values decreased to zero before 72 h, resulting in termination of the experiment before the corresponding time point could be evaluated reliably. The reported p-values represent the overall one-way ANOVA results.
BEAS-2B, non-tumorigenic bronchial epithelial cells; QUER, quercetin; ANOVA, analysis of variance; NSCLC, non-small cell lung cancer.

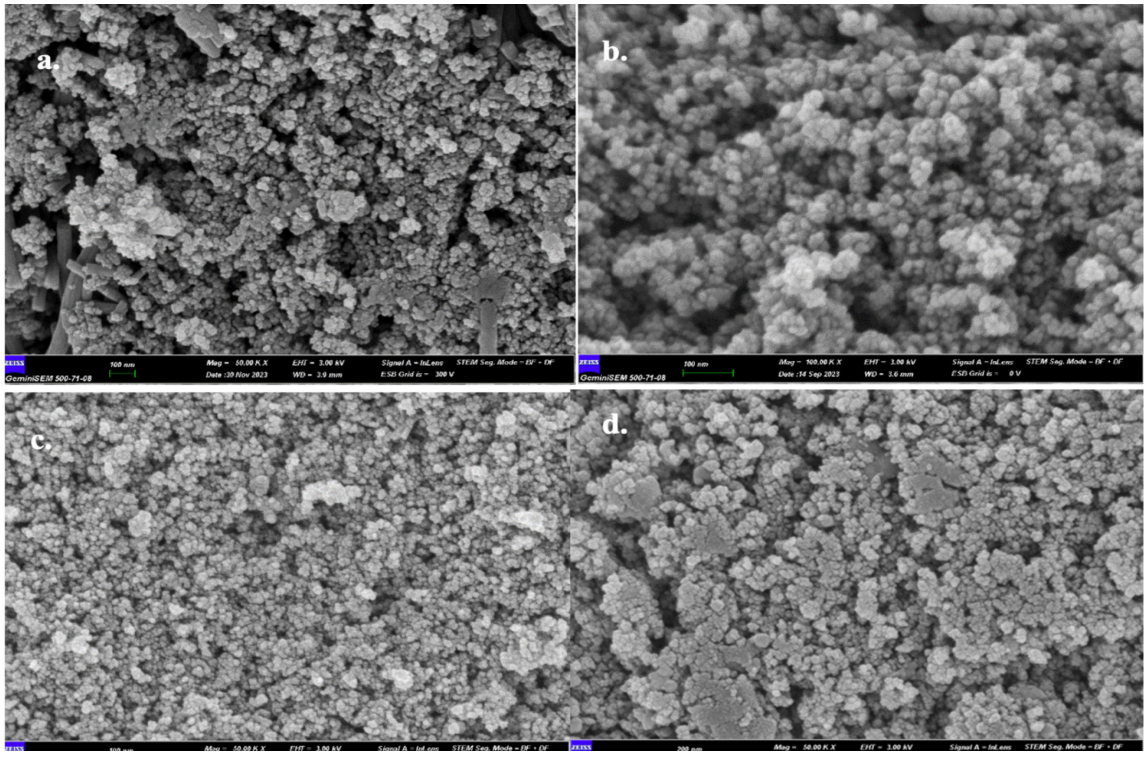


Figure 5. SEM images of the nanoparticle formulations: **a.** Fe_3O_4 (scale bar: 100 nm); **b.** Fe_3O_4 PEG (scale bar: 200 nm and 100 nm); **c.** Fe_3O_4 QUER (scale bar: 100 nm); and **d.** Fe_3O_4 -PEG-QUER (scale bar: 200 nm).

SEM, scanning electron microscopy; QUER, quercetin.

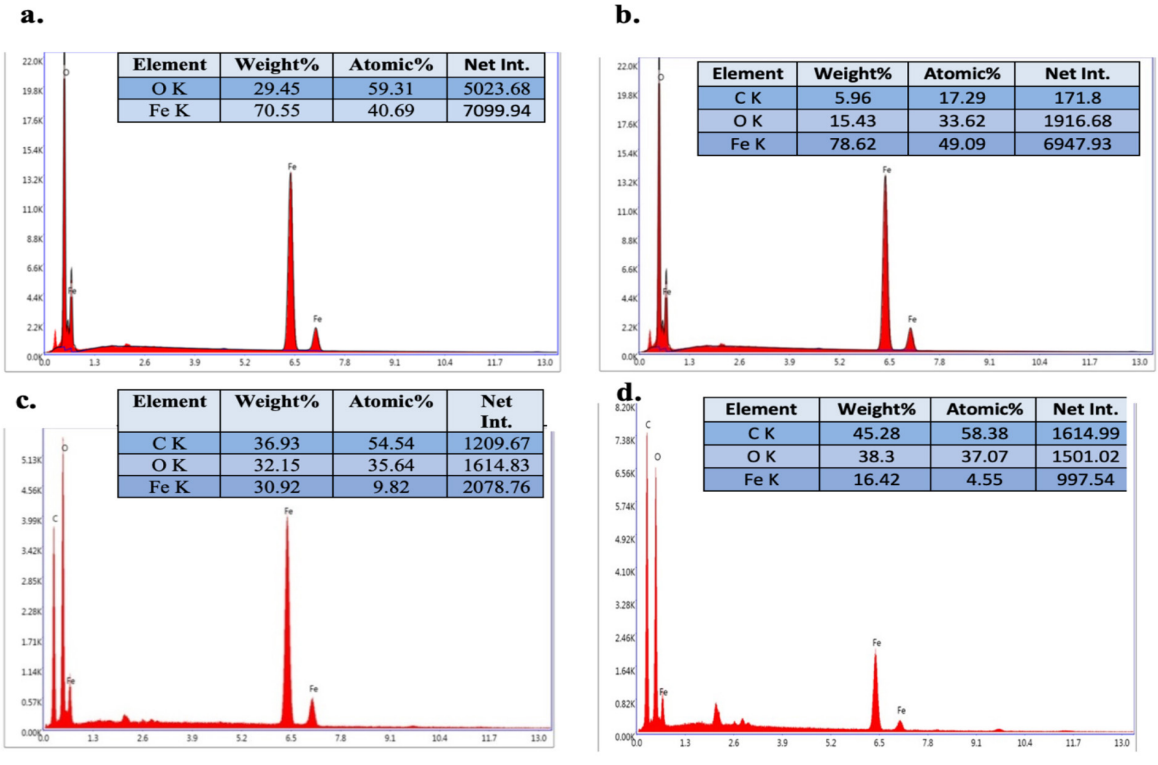


Figure 6. EDX spectra of the nanoparticle formulations: **a.** Fe_3O_4; **b.** Fe_3O_4-PEG; **c.** Fe_3O_4-QUER; and **d.** Fe_3O_4-PEG-QUER.

EDX, energy-dispersive X-ray spectroscopy; QUER, quercetin.

Overall, Fe_3O_4-PEG and Fe_3O_4-PEG-QUER produced measurable cytotoxic responses in A549 cells, whereas responses in BEAS-2B cells generally occurred at higher concentrations. Statistical comparisons with untreated controls were significant for the tested conditions ($p < 0.0001$).

Synthesized formulations were applied to cells in the concentration range of 12.5–400 µg/mL, and their effects were monitored for 48–72 hours using a time-dependent real-time xCELLigence system. As shown in the xCELLigence results tables, the cytotoxicity profiles differed between A549 and BEAS-2B cell lines. Because this is a real-time analysis, the graphs allow the toxicity profiles to be compared over time (Figure 7).

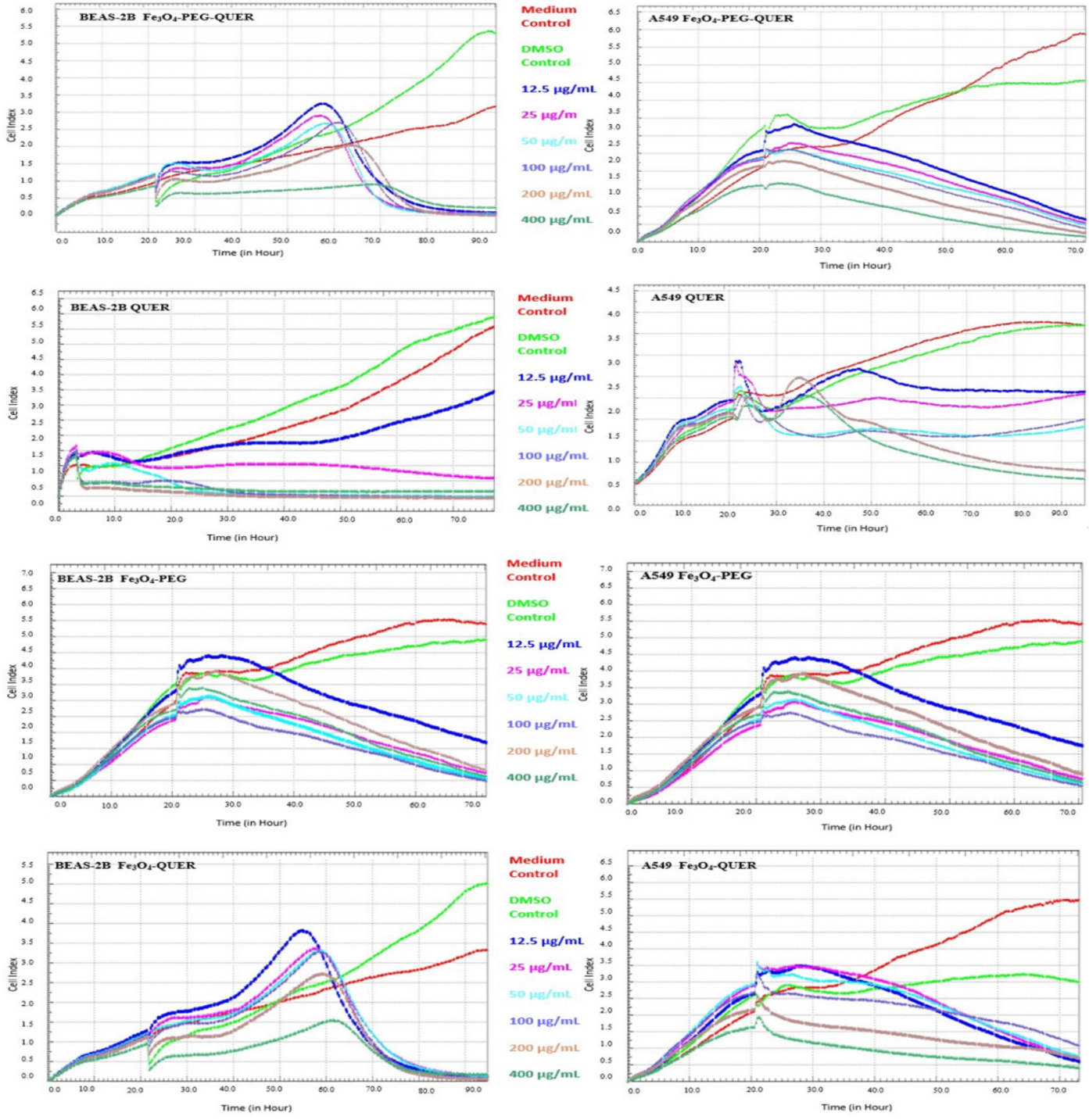


Figure 7. Real-time monitoring of the effects of Fe_3O_4-PEG, Fe_3O_4-QUER, Fe_3O_4-PEG-QUER, and free quercetin (QUER) on BEAS-2B and A549 cells using the xCELLigence system at 48 and 72 h.

BEAS-2B, non-tumorigenic bronchial epithelial cells.

The selectivity index (SI), calculated as the ratio of the IC50 value in BEAS-2B cells to that in A549 cells, was used to describe the relative difference in response between the two cell lines. SI values greater than 1 indicate a higher relative IC50 in BEAS-2B cells than in A549 cells, whereas values below 1 indicate a lower relative IC50 in BEAS-2B cells than in A549 cells. The SI values calculated for the tested formulations at 24, 48, and 72 h are presented in Table 4.

DISCUSSION

Magnetic IONP are particularly important in diseases due to oxidative damage.[46,47] However, there are several factors that strongly affect the antioxidant activity of nanomaterials, such as chemical composition, surface charge, particle size, and coating of the surface.[48-50] The surface coating can be biocompatible, non-toxic, and allow targeted drug delivery.[51,52]

In biomedical applications where MNP are used, stable, biocompatible nanoparticles are obtained by coating metals and metal oxides with a polymer. Fe in iron-oxide nanoparticles is reversibly used by cells.[53,54]

PEG, PVA and polyvinylpyrrolidone; superparamagnetic Fe_3O_4 material coated with coatings such as peptide, carbohydrate or protein facilitates drug loading and controlled release.[55]

Cancer is one of the leading causes of death, and the number of cancer-related deaths is increasing over time. Whether nanostructures can have an anticancer effect on the targeted area is a difficult research; many researchers have integrated commercial anticancer drugs into magnetite.[56,57] Drug systems integrated into this magnetite face challenges such as poor solubility, poor circulation in the bloodstream, and reduced drug clearance. Therefore, an effective drug delivery mechanism must be formulated to overcome such problems.[58] Quercetin is a widely known flavonoid found in fruits and vegetables.[59,60] Quercetin can be used in many fields as anticancer, anti-inflammatory, and antioxidant.[61] In addition to these areas of use, it has anticancer properties; It has high effectiveness on colon, breast and lung cancer.[62] More recently, quercetin-containing PEG-coated magnetic iron-oxide nanoparticles have also been investigated for their potential anti-tumor effects in cancer cells.[63] The present study was designed to examine a quercetin-containing Fe_3O_4 formulation *in vitro*. Similarly, the physicochemical properties of quercetin-containing Fe_3O_4 nanoparticles are suitable for use as an anticancer agent.[64] This provided the rationale for investigating an Fe_3O_4-based formulation containing PEG and quercetin, and for evaluating its *in vitro* effects on A549 and BEAS-2B cells.

The sizes and shapes of MNP vary depending on the method of synthesis. If MNP are synthesized in non-aqueous environments such as solvothermal, microwave and thermal decomposition methods, they are not suitable for use in the field of bio-application because they are hydrophobic.[57] Hydrophilic, cost-effective and environmentally friendly MNP can be synthesized by the precipitation method, which is easy to synthesize.[65] However, MNP obtained with this method has limitations such as not having a homogeneous size distribution and low stability.[66]

In their IONP (Fe_3O_4) synthesis, Jarzebski et al.[67] found an average peak of 208 nm and the most intense peak of 154 nm in the NTA results. (They used a laser beam with a wavelength of 405 nm). In this study, the mean particle size was determined to be 99.1 nm, while the most intense peak was observed at 54.6 nm. Thus, the particle size falls within the 1–100 nm range generally defined for nanoparticles. If we could control the size of our formulation, we could achieve an average size of approximately 54.6 nm, which corresponds to the strongest peak. Using the Microfluidics M110P device, we were able to further reduce particle sizes under high pressure.

Nurbas et al.[68] synthesized IONP from $FeCl_2.4H_2O$:$FeCl_3.6H_2O$ (2:1) and added NaOH to the medium instead of NH_3. They found the Zeta potential of NP, which they obtained with a size of approximately 35 nm, to be -24.80 mV. The value found is more negative than that of the IONP synthesized in this study, although the IONP has a smaller particle size. If they had applied the NP they synthesized to the cell, they would likely have obtained better results, since the particle size was smaller than that of the NP we obtained. Since the zeta potential of the IONP synthesized in this study is -9.74 mV, this may have contributed to the observed cellular response through interactions with the cellular environment.

Verma et al.[49] synthesized IONP from $FeCl_2$ and $FeCl_3$ using 0.4 M HCl and 0.5 M NaOH, and attached Quercetin and PLGA to IONP. They administered PLGA-MNP and MNP at dosages of 10–250 µg/mL to the A549 cell line and analyzed the cells with xCELLigence (Roche). They observed that the MNP they applied reduced the cell index slightly, whereas MNP coated with PLGA did not cause a significant change. According to TEM, they found

Table 4. Selectivity index (SI) values of Fe_3O_4-based formulations and free quercetin in A549 and BEAS-2B cells at 24,48 and 72 h.

Formulation	SI 24 h*	SI 48 h*	SI 72 h*
Fe_3O_4-PEG	14.59	20.74	N/D
Fe_3O_4-QUER	> 2.48	0.93	N/D
Fe_3O_4-PEG-QUER	> 1.38	> 2.50	N/D
Free quercetin	1.00	1.00	0.18

*SI. SI was calculated as the ratio of the IC50 value in BEAS-2B cells to that in A549 cells at the corresponding time point (SI = IC50, BEAS-2B / IC50, A549). Values preceded by ">" indicate that the IC50 value in BEAS-2B cells was not reached within the tested concentration range and therefore represent a lower limit of the SI. N/D indicates that the corresponding IC50 value was not determined; see the IC_{50} table footnote for the experimental reason.
BEAS-2B, non-tumorigenic bronchial epithelial cells; QUER, quercetin.

the MNP particle size they produced to be approximately 9 nm, and the MNP-PLGA size to be approximately 54 nm.[49] Although the size of the PLGA-coated particles they produced and the methods used to measure size differed from those of our MNP-PEG formulation, we can say that the observed response at a lower concentration under the tested conditions, relative to our formulation, may be associated with it being smaller in size. Since PLGA is a negatively charged polymer, it may have increased the negative charge of the magnetite, making cellular entry difficult. In our study, when neutral PEG was used, the magnetite shifted to the neutral area and therefore the 24-hour IC50 and 48-hour IC50 values for the A549 cell line were approximately 27-19 µg/mL, respectively. It was effective at very small doses.

Study limitations

Several limitations should be considered when interpreting the findings of this study. The amount of quercetin associated with the Fe_3O_4-PEG-QUER formulation was not quantitatively determined; consequently, quercetin loading efficiency, encapsulation efficiency, recovery yield, and release kinetics could not be established. The available physicochemical characterization techniques did not allow a definitive determination of the molecular nature of the interaction between Fe_3O_4, PEG, and quercetin; therefore, covalent conjugation should not be inferred from the present data.

Cytotoxicity experiments were performed using total formulation concentrations, which precluded direct comparisons of quercetin-equivalent doses. The maximum concentration tested was 400 µg/mL, and IC50 values above this concentration were therefore considered › 400 µg/mL. The original experimental design did not include a bare Fe_3O_4 treatment group, nanoparticle-only impedance controls, or an orthogonal viability assay. The absence of nanoparticle-only impedance controls limited the assessment of potential particle-related interference with the impedance-based measurements, while the lack of an orthogonal viability assay prevented independent confirmation of the observed cellular responses. In addition, the final DMSO concentration varied across the tested formulation concentrations, and concentration-matched vehicle controls were not included at each dose. Therefore, a potential contribution of DMSO to the observed cellular responses cannot be excluded.

Collectively, these findings provide preliminary *in vitro* evidence of the physicochemical characteristics and cellular responses of Fe_3O_4-PEG-QUER and warrant further investigation in appropriate experimental models. The observed cellular responses should not be interpreted as evidence of established safety, targeted delivery, enhanced cellular uptake, or therapeutic efficacy. The current study is limited to in vitro experiments; further studies incorporating complementary cellular assays, appropriate nanoparticle controls, quantitative quercetin analysis, and characterization under biologically relevant conditions are needed to address these limitations. Further *in vivo* and, subsequently, clinical investigations would be required to establish the therapeutic potential of these formulations.

CONCLUSION

In the present study, a ternary Fe_3O_4-PEG-QUER nanoparticle formulation was synthesized via the coprecipitation method. A nanoscale formulation was designed to combine Fe_3O_4, PEG, and quercetin. Comprehensive characterization using XRD, FT-IR, NTA, Zeta-sizer, SEM, and EDX provided complementary information on the physicochemical properties of the four formulations.

XRD confirmed the presence of the inverse spinel cubic crystal structure in the Fe_3O_4-containing formulations. FT-IR provided information on the characteristic functional groups associated with PEG and quercetin. NTA showed that Fe_3O_4-PEG-QUER had a mean particle diameter in the sub-100 nm range under the measurement conditions. Zeta potential analysis showed that the PEG-containing formulation exhibited a near-neutral surface charge, which may influence cellular interactions. SEM showed predominantly spherical particle morphology, while EDX provided information on the elemental composition of the formulations.

In vitro assessment of impedance-based cellular responses using the xCELLigence system demonstrated differential impedance profiles between A549 NSCLC and BEAS-2B cells under the tested conditions. The apparent IC50 values for Fe_3O_4-PEG-QUER in A549 cells were 289 µg/mL at 24 h and 160 µg/mL at 48 h, whereas those exceeded 400 µg/mL. Notably, Fe_3O_4-PEG alone exhibited lower apparent IC50 values in A549 cells than Fe_3O_4-PEG-QUER did, indicating that the addition of quercetin did not enhance the observed antiproliferative response under the present experimental conditions. Because the concentrations were expressed as total formulation mass and the quercetin content of Fe_3O_4-PEG-QUER was not quantitatively determined, the observed responses could not be directly compared at equivalent quercetin doses. These findings represent preliminary *in vitro* observations and do not establish the safety, targeted delivery, enhanced cellular uptake, or therapeutic efficacy of the formulations. Further studies using complementary cellular assays and appropriate experimental models are needed to clarify the contribution of quercetin to the observed effects and to investigate the potential of these formulations.

Ethics

Ethics Committee Approval: There are no circumstances requiring ethics committee approval for this study.

Informed Consent: Since only *in vitro* experiments were conducted within the scope of this study, patient consent was not required.

Footnotes

Authorship Contributions

Concept: Y.S., M.B.Y., Design: Y.S., M.B.Y., Data Collection or Processing: Y.S., M.B.Y., Analysis or Interpretation: Y.S., M.B.Y., Literature Search: Y.S., M.B.Y., Writing: Y.S., M.B.Y.

Conflict of Interest: The authors declare no conflicts of interest.

Financial Disclosure: This study was supported by Erciyes University Scientific Research Projects Coordination Unit (BAP) under Project No. (TYL-2023-12897).

REFERENCES

1. Gubbala S, Nathani H, Koizol K, Misra RDK. Magnetic properties of nanocrystalline Ni–Zn, zn–mn, and ni–mn ferrites synthesized by reverse micelle technique. Physica B: Condensed Matter. 2004;348:317-328.
2. Arruebo M, Fernández-Pacheco R, Ibarra MR, Santamaría J. Magnetic nanoparticles for drug delivery. Nano Today. 2007;2:22-32.
3. Rana S, Philip J, Raj B. Micelle based synthesis of cobalt ferrite nanoparticles and its characterization using Fourier transform infrared transmission spectrometry and thermogravimetry. Materials Chemistry and Physics. 2010;124:264-269.
4. McBain SC, Griesenbach U, Xenariou S, Keramane A, Batich CD, Alton EW, Dobson J. Magnetic nanoparticles as gene delivery agents: enhanced transfection in the presence of oscillating magnet arrays. Nanotechnology. 2008;19:405102.
5. Laurent S, Forge D, Port M, Roch A, Robic C, Vander Elst L, Muller RN. Magnetic iron oxide nanoparticles: synthesis, stabilization, vectorization, physicochemical characterizations, and biological applications. Chem Rev. 2008;108:2064-2110.
6. Dobson J. Magnetic nanoparticles for drug delivery. Drug Development Research. 2006;67:55-60.
7. Veiseh O, Gunn JW, Zhang M. Design and fabrication of magnetic nanoparticles for targeted drug delivery and imaging. Adv Drug Deliv Rev. 2010;62:284-304.
8. Karakoti AS, Das S, Thevuthasan S, Seal S. PEGylated inorganic nanoparticles. Angew Chem Int Ed Engl. 2011;50:1980-1994.
9. Mukhopadhyay A, Joshi N, Chattopadhyay K, De G. A facile synthesis of PEG-coated magnetite (Fe3O4) nanoparticles and their prevention of the reduction of cytochrome c. ACS Appl Mater Interfaces. 2012;4:142-149.
10. Ahmed MA, Okasha N, Mansour SF, El-dek SI. Bi-modal improvement of the physico-chemical characteristics of peg and Mfe2o4 subnanoferrite. Journal of Alloys and Compounds. 2010;496:345-350.
11. Feng B, Hong RY, Wang LS, Guo L, Li HZ, Ding J, Zheng Y, Wei DG. Synthesis of Fe_3O_4/APTES/Peg diacid functionalized magnetic nanoparticles for MR imaging. Colloids and Surfaces A: Physicochemical and Engineering Aspects. 2008;328:52-59.
12. Zhang Y, Kohler N, Zhang M. Surface modification of superparamagnetic magnetite nanoparticles and their intracellular uptake. Biomaterials. 2002;23:1553-1561.
13. Sainz V, Conniot J, Matos AI, Peres C, Zupancic E, Moura L, Silva LC, Florindo HF, Gaspar RS. Regulatory aspects on nanomedicines. Biochem Biophys Res Commun. 2015;468:504-510.
14. McCarthy JR, Weissleder R. Multifunctional magnetic nanoparticles for targeted imaging and therapy. Adv Drug Deliv Rev. 2008;60:1241-1251.
15. Petros RA, DeSimone JM. Strategies in the design of nanoparticles for therapeutic applications. Nat Rev Drug Discov. 2010;9:615-627.
16. Peer D, Karp JM, Hong S, Farokhzad OC, Margalit R, Langer R. Nanocarriers as an emerging platform for cancer therapy. Nat Nanotechnol. 2007;2:751-760.
17. Cornell RM, Schwertmann U. The iron oxides. 2003.
18. Gossuin Y, Gillis P, Hocq A, Vuong QL, Roch A. Magnetic resonance relaxation properties of superparamagnetic particles. Wiley Interdiscip Rev Nanomed Nanobiotechnol. 2009;1:299-310.
19. Schwertmann U. Solubility and dissolution of iron oxides. Plant and Soil. 1991;130;1-25.
20. Macdougall IC. Evolution of iv iron compounds over the last century. J Ren Care. 2009;35(Suppl 2):8-13.
21. Danielson BG. Structure, chemistry, and pharmacokinetics of intravenous iron agents. J Am Soc Nephrol. 2004;15(Suppl 2):S93-S98.
22. Gupta AK, Gupta M. Synthesis and surface engineering of iron oxide nanoparticles for biomedical applications. Biomaterials. 2005;26:3995-4021.
23. Wang YX, Hussain SM, Krestin GP. Superparamagnetic iron oxide contrast agents: physicochemical characteristics and applications in MR imaging. Eur Radiol. 2001;11:2319-2331.
24. Na HB, Song IC, Hyeon T. Inorganic nanoparticles for MRI contrast agents. Advanced Materials, 2009;21:2133-2148.
25. Panche AN, Diwan AD, Chandra SR. Flavonoids: an overview. J Nutr Sci. 2016;5:e47.
26. Zheng X, Zhang X, Zeng F. Biological functions and health benefits of flavonoids in fruits and vegetables: a contemporary review. Foods. 2025;14:155.
27. Lee YK, Yuk DY, Lee JW, Lee SY, Ha TY, Oh KW, Yun YP, Hong JT. (-)-Epigallocatechin-3-gallate prevents lipopolysaccharide-induced elevation of beta-amyloid generation and memory deficiency. Brain Res. 2009;1250:164-174.
28. Metodiewa D, Kochman A, Karolczak S. Evidence for antiradical and antioxidant properties of four biologically active N,N-diethylaminoethyl ethers of flavanone oximes: a comparison with natural polyphenolic flavonoid (rutin) action. Biochem Mol Biol Int. 1997;41:1067-1075.
29. Walker EH, Pacold ME, Perisic O, Stephens L, Hawkins PT, Wymann MP, Williams RL. Structural determinants of phosphoinositide 3-kinase inhibition by wortmannin, LY294002, quercetin, myricetin, and staurosporine. Mol Cell. 2000;6:909-919.
30. Wink M. Phytochemical diversity of secondary metabolites. Encyclopedia of Plant and Crop Science. 2004;915-919.
31. Pal D, Nayak KA. Nanotechnology for targeted delivery in cancer therapeutics. Int J Pharm Sci Rev Res. 2010;1:1-10.
32. Ferlay J, Soerjomataram I, Dikshit R, Eser S, Mathers C, Rebelo M, Parkin DM, Forman D, Bray F. Cancer incidence and mortality worldwide: sources, methods and major patterns in GLOBOCAN 2012. Int J Cancer. 2015;136:E359-E386.
33. Auyang YS. Cancer causes and cancer research on many levels of complexity. Creat Technol. 2006:1-15.
34. Singh KK. Nanotechnology in cancer detection and treatment. Technology in Cancer Research and Treatment. 2005;4:583-583.
35. Singh PO, Nehru MR. Nanotechnology and cancer treatment. Asian J Exp Sci. 2008;22:6.
36. Anselmo AC, Mitragotri S. Nanoparticles in the clinic. Bioeng Transl Med. 2016;1:10-29.
37. Barenholz Y. Doxil®--the first FDA-approved nano-drug: lessons learned. J Control Release. 2012;160:117-134.
38. Yoo E, Cheng HA, Nardacci LE, Beaman DJ, Drinnan CT, Lee C, Fishbein KW, Spencer RG, Fisher OZ, Doiron AL. Activatable interpolymer complex-superparamagnetic iron oxide nanoparticles as magnetic resonance contrast agents sensitive to oxidative stress. Colloids and Surfaces B: Biointerfaces. 2017;158:578-588.
39. Shah ST, Yehye WA, Chowdhury ZZ, Simarani K. Magnetically directed antioxidant and antimicrobial agent: synthesis and surface functionalization of magnetite with quercetin. PeerJ. 2019;7:e7651.

40. Shah ST, A Yehya W, Saad O, Simarani K, Chowdhury Z, A Alhadi A, Al-Ani LA. Surface functionalization of ıron oxide nanoparticles with gallic acid as potential antioxidant and antimicrobial agents. Nanomaterials (Basel). 2017;7:306.

41. Bukhari SB, Memon S, Mahroof-Tahir M, Bhanger MI. Synthesis, characterization and antioxidant activity copper-quercetin complex. Spectrochim Acta A Mol Biomol Spectrosc. 2009;71:1901-1906.

42. Kumar SR, Priyatharshni S, Babu VN, Mangalaraj D, Viswanathan C, Kannan S, Ponpandian N. Quercetin conjugated superparamagnetic magnetite nanoparticles for in-vitro analysis of breast cancer cell lines for chemotherapy applications. J Colloid Interface Sci. 2014;436:234-242.

43. Cheng HA, Drinnan CT, Pleshko N, Fisher OZ. Pseudotannins self-assembled into antioxidant complexes. Soft Matter. 2015;11:7783-7791.

44. Dorniani D, Kura AU, Hussein-Al-Ali SH, Bin Hussein MZ, Fakurazi S, Shaari AH, Ahmad Z. In vitro sustained release study of gallic acid coated with magnetite-PEG and magnetite-PVA for drug delivery system. ScientificWorldJournal. 2014;2014:416354.

45. Rosman R, Saifullah B, Maniam S, Dorniani D, Hussein MZ, Fakurazi S. Improved anticancer effect of magnetite nanocomposite formulation of GALLIC acid (Fe_3O_4-PEG-GA) against lung, breast and colon cancer cells. Nanomaterials (Basel). 2018;8:83.

46. Zhu J, Wang J, Wang X, Zhu J, Yang Y, Tian J, Cui W, Ge C, Li Y, Pan Y, Gu H. Facile synthesis of magnetic core–shell nanocomposites for MRI and CT bimodal imaging. Journal of Materials Chemistry B. 2015;3:6905-6910.

47. Chorny M, Hood E, Levy RJ, Muzykantov VR. Endothelial delivery of antioxidant enzymes loaded into non-polymeric magnetic nanoparticles. J Control Release. 2010;146:144-151.

48. Song G, Zhao M, Chen H, Lenahan C, Zhou X, Ou Y, He Y. The role of nanomaterials in stroke treatment: targeting oxidative stress. Oxid Med Cell Longev. 2021;2021:8857486.

49. Verma NK, Crosbie-Staunton K, Satti A, Gallagher S, Ryan KB, Doody T, McAtamney C, MacLoughlin R, Galvin P, Burke CS, Volkov Y, Gun'ko YK. Magnetic core-shell nanoparticles for drug delivery by nebulization. J Nanobiotechnology. 2013;11:1.

50. Cîrcu M, Nan A, Borodi G, Liebscher J, Turcu R. Refinement of magnetite nanoparticles by coating with organic stabilizers. Nanomaterials (Basel). 2016;6:228.

51. Santiago-Rodríguez L, Lafontaine MM, Castro C, Méndez-Vega J, Latorre-Esteves M, Juan EJ, Mora E, Torres-Lugo M, Rinaldi C. Synthesis, stability, cellular uptake, and blood circulation time of carboxymethyl-inulin coated magnetic nanoparticles. J Mater Chem B. 2013;1:2807-2817.

52. Lam T, Avti PK, Pouliot P, Maafi F, Tardif JC, Rhéaume É, Lesage F, Kakkar A. Fabricating water dispersible superparamagnetic iron oxide nanoparticles for biomedical applications through ligand exchange and direct conjugation. Nanomaterials (Basel). 2016;6:100.

53. Bulte JW, Kraitchman DL. Iron oxide MR contrast agents for molecular and cellular imaging. NMR Biomed. 2004;17:484-499.

54. Chomoucka J, Drbohlavova J, Huska D, Adam V, Kizek R, Hubalek J. Magnetic nanoparticles and targeted drug delivering. Pharmacol Res. 2010;62:144-149.

55. Reddy LH, Arias JL, Nicolas J, Couvreur P. Magnetic nanoparticles: design and characterization, toxicity and biocompatibility, pharmaceutical and biomedical applications. Chem Rev. 2012;112:5818-5878.

56. Yang XL, Ju XJ, Mu XT, Wang W, Xie R, Liu Z, Chu LY. Core-shell chitosan microcapsules for programmed sequential drug release. ACS Appl Mater Interfaces. 2016;8:10524-10534.

57. Ding G, Guo Y, Lv Y, Liu X, Xu L, Zhang X. A double-targeted magnetic nanocarrier with potential application in hydrophobic drug delivery. Colloids Surf B Biointerfaces. 2012;91:68-76.

58. Schladt TD, Schneider K, Schild H, Tremel W. Synthesis and bio-functionalization of magnetic nanoparticles for medical diagnosis and treatment. Dalton Trans. 2011;40:6315-6343.

59. Kumari A, Yadav SK, Pakade YB, Singh B, Yadav SC. Development of biodegradable nanoparticles for delivery of quercetin. Colloids Surf B Biointerfaces. 2010;80:184-192.

60. Wu TH, Yen FL, Lin LT, Tsai TR, Lin CC, Cham TM. Preparation, physicochemical characterization, and antioxidant effects of quercetin nanoparticles. Int J Pharm. 2008;346:160-168.

61. Chakraborty S, Stalin S, Das N, Choudhury ST, Ghosh S, Swarnakar S. The use of nano-quercetin to arrest mitochondrial damage and MMP-9 upregulation during prevention of gastric inflammation induced by ethanol in rat. Biomaterials. 2012;33:2991-3001.

62. Kakran M, Sahoo NG, Li L. Dissolution enhancement of quercetin through nanofabrication, complexation, and solid dispersion. Colloids Surf B Biointerfaces. 2011;88:121-130.

63. Tiburzi S, Lezcano V, Principe G, Montiel Schneider MG, Miravalles AB, Lassalle V, Bruzzone A, González-Pardo V. Quercetin-loaded magnetic nanoparticles: a promising tool for antitumor treatment in human breast cancer cells. J Drug Target. 2025;33:1227-1242.

64. Barreto ACH, Santiago VR, Mazzetto SE, Denardin JC, Lavín R, Mele G, Ribeiro ME, Vieira IG, Gonçalves T, Ricardo NM, Fechine PB. Magnetic nanoparticles for a new drug delivery system to control quercetin releasing for cancer chemotherapy. J Nanopart Res. 2011;13:6545-6553.

65. Pereira C, Pereira AM, Fernandes C, Rocha M, Mendes R, Fernández-García MP, Guedes A, Tavares PB, Grenèche J.-M, Araújo JP, Freire C. Superparamagnetic MFE_2O_4 (M = fe, co, MN) nanoparticles: tuning the particle size and magnetic properties through a novel one-step coprecipitation route. Chemistry of Materials. 2012;24:1496-1504.

66. Qu H, Ma H, Riviere A, Zhoub W, O'Connor JC. One-pot synthesis in polyamines for preparation of water-soluble magnetite nanoparticles with amine surface reactivity. J Mater Chem. 2012;22:3311-3319.

67. Jarzebski M, Kościński M, Bialopiotrowıcz T. Determining the size of nanoparticles in the example of magnetic iron oxide core-shell systems. Journal of Physics Conference Series. 2017;885:012007.

68. Nurbas M, Ghorbanpoor H, Avcı H. An eco-friendly approach to synthesis and characterization of magnetite (Fe_3O_4) nanoparticles using platanus orientalis l. Leaf extract. Digest Journal of Nanomaterials and Biostructures. 2017;12:993-1000.